Supplement of Atmos. Chem. Phys., 21, 15985–16000, 2021
https://doi.org/10.5194/acp-21-15985-2021-supplement

Supplement of

Winter $ClNO_2$ formation in the region of fresh anthropogenic emissions: seasonal variability and insights into daytime peaks in northern China

Men Xia et al.

Correspondence to: Tao Wang (cetwang@polyu.edu.hk)

Supplement of “Winter $ClNO_2$ formation in the region of fresh anthropogenic emissions: Seasonal variability and insights into daytime peaks in northern China” by Men Xia et al.,

Table of Contents

Table captions

Figure captions

References

Section S1: technical details of N_2O_5 and $ClNO_2$ measurements

The detailed principle and description of technical aspects of the Q-CIMS, e.g., measures to minimize the inlet interference of N_2O_5 and $ClNO_2$, are available in the previous studies (Tham et al., 2016; Wang et al., 2016; Xia et al., 2020). Here we present the isotopic analysis of $ClNO_2$ signals and the normalized sensitivity of N_2O_5 and $ClNO_2$.

S1.1. Identification of $ClNO_2$ and N_2O_5

The primary ions, I^- and $I(H_2O)^-$, were recorded at 127 atomic mass unit (a.m.u.) (Fig. S2b) and 145 a.m.u. (Fig. S2c), respectively. The analytes, $ClNO_2$ and N_2O_5, were recognized as $I^{35}ClNO_2^-$ (208 a.m.u., Fig. S2d), $I^{37}ClNO_2^-$ (210 a.m.u., Fig. S2d), and $IN_2O_5^-$ (235 a.m.u.), respectively on the Q-CIMS spectrum. Before each campaign, we calibrated the mass so that the peak of N_2O_5 and $ClNO_2$ signals points to 235.0 and 208.0. Manual scans of the mass spectrum (30~300 a.m.u.) were performed every day during the ambient sampling, in which the signals of I^-, $I(H_2O)^-$, $I^{35}ClNO_2^-$, $I^{37}ClNO_2^-$, and $IN_2O_5^-$ were recorded. The daily manual check of the peak shape and peak position ensures accurate identifications of the primary ions and analytes in this study. To further ensure the identity of $ClNO_2$, we compared the ratio of 208 a.m.u. and 210 a.m.u. signals during the ambient sampling and calibrations (Fig. S3). As for N_2O_5, field measurements at a rural site north of Beijing with a higher mass resolution spectrometer (HR-ToF-CIMS) showed no interference from other chemicals (Breton et al., 2018). However, a recent study revealed that hydroperoxymethyl thioformate, an oxidation product of dimethyl sulfide (DMS) by OH, does overlap with the N_2O_5 signal at 235 a.m.u in their iodide HR-ToF-CIMS (Veres et al., 2020). This interference was negligible at our three sites due to very low daytime signals of 235 a.m.u., typically below 15 pptv by assuming all 235 a.m.u. signals were N_2O_5. This result is consistent with anticipated low concentrations of DMS at our inland sites.

S1.2. Quantification of $ClNO_2$ and N_2O_5

This section presents the sensitivity issues, detection limits, and uncertainty analysis of the Q-CIMS measurements. The detection limits of $ClNO_2$ and N_2O_5 (3σ, 5-min) are shown in Table S1. A detailed description of the uncertainty of N_2O_5 and $ClNO_2$ measurements (~19 %) is available in Xia et al. (2020). The sensitivity issues are introduced as follows.

On-site calibrations of $ClNO_2$ and N_2O_5 are referred to section 2.2 in the main text. The mixing ratios of $ClNO_2$ and N_2O_5 were calculated using the normalized sensitivity, which is essential to compensate for the potential changes in primary ions. The normalized sensitivity of $ClNO_2$ and N_2O_5 is defined as the signal ratio of 208 a.m.u. to 145 a.m.u. ($I(H_2O)^-$) and 235 a.m.u. to 145 a.m.u. in the presence of 1-pptv $ClNO_2$ or N_2O_5, respectively. For example, a normalized sensitivity of 1.3×10^{-5} $pptv^{-1}$ of N_2O_5 indicates that the sensitivity of N_2O_5 is 1.3 Hz/pptv in the presence of 10^5 Hz of $I(H_2O)^-$ signals. The normalized sensitivities of $ClNO_2$ ($(0.9 - 1.8) \times 10^{-5}$ $pptv^{-1}$) and N_2O_5 ($(1.3 - 2.2) \times 10^{-5}$ $pptv^{-1}$) are stable within each campaign (Fig. S5). A discrepancy of normalized sensitivities of $ClNO_2$ and N_2O_5 exists among different campaigns, owing to unknown factors, e.g., changes of instrument status after transport. We found a negative dependence of the normalized sensitivity of N_2O_5 on RH during the on-site calibrations (Fig. S4). While there is no obvious dependence of the normalized sensitivity of $ClNO_2$ on RH.

Table S1. Integration time of the signals recorded by the Q-CIMS in the winter campaigns.

Mass to charge ratio	Integration time (ms)	Mass to charge ratio	Integration time (ms)
62	287	210	287
145	587	217	287
163	290	222	290
165	287	223	287
173	287	234	286
174	287	235	1237
178	287	241	287
179	287	243	287
192	287	245	287
197	287	254	287
199	288	280	287
207	287	287	287
208	1239	289	288
209	287	291	287
Total integration time		10.2 s	

Table S2. Sensitivities and detection limits of N_2O_5 and $ClNO_2$ measurements.

Site	Wangdu	Beijing	Mt. Tai
Detection limit of N_2O_5[1]	7.3 ± 1.0	6.9 ± 1.6	6.9 ± 2.3
Detection limit of $ClNO_2$[1]	5.3 ± 1.3	3.9 ± 1.9	3.8 ± 1.9
Normalized sensitivity of N_2O_5[2]	$(1.3 \pm 0.2) \times 10^{-5}$	$(2.2 \pm 0.2) \times 10^{-5}$	$(1.7 \pm 0.2) \times 10^{-5}$
Normalized sensitivity of $ClNO_2$[2]	$(9.1 \pm 1.9) \times 10^{-6}$	$(1.8 \pm 0.2) \times 10^{-5}$	$(1.4 \pm 0.2) \times 10^{-5}$

[1] The detection limits (unit: pptv) are derived from the standard deviations of the signals (3σ in 5-min data) in the background testing.

[2] The unit for the normalized sensitivity is $pptv^{-1}$.

Table S3. The measured species and instruments in the field campaigns.

Measured species	Instruments	Detection limits	Time resolution
N_2O_5, $ClNO_2$	Q-CIMS, THS	5~8 pptv	10 s
NO, NO_2	42i-TL, Thermo Scientific	0.06 ppbv	1 min

NO_y	EC9843, Ecotech	0.1 ppbv	1 min
CO	48i, Thermo Scientific	4 ppbv	1 min
SO_2	43C, Thermo Scientific	0.1 ppbv	1 min
O_3	49i, Thermo Scientific	0.5 ppbv	1 min
HONO	LOPAP-03, QUMA	5 pptv	1 min
jNO_2	Filter Radiometer, metcon	4×10^{-5} s^{-1}	10 s
$PM_{2.5}$	TEOM 1400A, Thermo Scientific	1 μg m^{-3}	1 min
VOCs	GC-MS/FID, Chromatotec Group	~10 pptv	1 h
PNSD	WPS 1000XP, MSP Corp.	1 particle cm^{-3}	1 min
NH_4^+, Cl^-, NO_3^-, SO_4^{2-}	ACSM, Aerodyne Research Inc.	0.01~0.06 μg m^{-3}	10 min
	MARGA, Metrohm AG	0.01~0.06 μg m^{-3}	1 h

Table S4. Input parameters of the box model for case studies with high concentrations of daytime $ClNO_2$.

No.	Parameter	Wangdu[1]	Beijing[1]	Mt. Tai[1]
1	$PM_{2.5}$ (μg m^{-3})	162.23±90.64	116.47±69.33	66.65±37.11
2	RH (%)	69.22±7.67	33.78±14.67	85.52±14.43
3	Temp (°C)	-1.95±2.77	1.43±4.17	9.88±1.53
4	NO (ppbv)	87.84±89.48	25.62±27.52	0.36±0.35
5	NO_2 (ppbv)	39.58±7.68	37.24±19.28	3.83±2.04
6	O_3 (ppbv)	3.74±2.71	12.37±10.57	59.79±8.6
7	CO (ppbv)	3156.92±1240.79	1881.1±898.67	623.8±213.84
8	SO_2 (ppbv)	11.87±3.28	6.22±2.25	2.13±1.85
9	N_2O_5 (ppbv)	0.02±0.01	0.07±0.11	0.01±0.02
10	$ClNO_2$ (ppbv)	0.33±0.28	0.16±0.17	0.26±0.21
11	HONO (ppbv)	4.13±2.41	1.02±0.46	0.13±0.09
12	jNO_2 ($\times10^{-3}$ s^{-1})	0.59±0.86	0.95±1.43	0.88±1.23
13	Ethane	16.13±8	0.96±0.42	3.93±0.45
14	Ethene	1.93±1.42	0.43±0.18	1.1±0.53
15	Propane	6.48±2.96	6.03±0.9	1.94±0.52
16	Propene	5.53±4.27	2.02±0.81	0.15±0.09
17	i-Butane	1.93±0.51	0.79±0.28	0.39±0.16
18	n-Butane	3.84±1.14	1.18±0.69	0.74±0.33
19	Ethyne	6.04±3.53	0.38±0.36	2.1±0.32
20	trans-2-Butene	0.27±0.26	-	0.01±0.01
21	1-Butene	0.77±0.61	0.04±0.01	0.03±0.02
22	cis-2-Butene	0.14±0.05	0.15±0.04	0.01±0.01
23	Cyclopentane	2.67±0.7	0.02±0	0.04±0.02
24	i-Pentane	0.21±0.17	-	0.35±0.18

25	n-Pentane	1.53±0.51	-	0.25±0.11
26	Freon114	0.03±0	-	0.02±0
27	Chloromethane	0.45±0.06	-	1.1±0.31
28	1,3-Butadiene	0.27±0.23	0.04±0.01	0.02±0.01
29	Bromomethane	0.01±0	-	0.06±0.06
30	Freon11	0.4±0.04	-	0.26±0.01
31	1-Pentene	0.18±0.15	0.02±0.01	0.01±0.01
32	trans-2-Pentene	0.14±0.11	-	-
33	Isoprene	0.13±0.12	0.01±0	0.01±0.01
34	Freon113	0.07±0	0.07±0	0.08±0
35	Dichloromethane	1.64±0.98	-	0.45±0.08
36	2-Methylpentane	0.44±0.15	-	0.06±0.03
37	3-Methylpentane	0.36±0.09	-	0.04±0.02
38	2,2-Dimethylbutane	0.05±0.01	-	-
39	2,3-Dimethylbutane	0.07±0.03	-	-
40	n-hexane	0.62±0.23	0.22±0.05	0.09±0.05
41	2-Propenal	0.03±0.02	0.13±0	2.91±1.29
42	2,4-Dimethylpentane	-	-	-
43	Chloroform	0.66±0.21	-	0.32±0.14
44	Methyl chloroform	0.01±0	-	0±0
45	Carbon tetrachloride	0.15±0.01	-	0.11±0.02
46	Cyclohexane	0.18±0.05	0.33±0.16	-
47	3-Methylhexane	-	0.03±0.01	-
48	Methyl tert-butyl ether	0.16±0.05	-	-
49	Benzene	4.25±2.63	1.58±0.37	0.71±0.19
50	2,2,4-Trimethylpentan	0.07±0.03	-	0.02±0.01
51	n-Heptane	0.24±0.13	0.06±0.03	0.04±0.02
52	Toluene	3.28±1.58	0.61±0.31	0.37±0.24
53	n-Octane	0.17±0.1	0.06±0.04	0.03±0.01
54	Ethylbenzene	0.47±0.25	0.14±0.07	0.09±0.03
55	n-Nonane	0.13±0.09	0.01±0.01	0.04±0.02
56	m-Xylene	1.15±0.65	0.29±0.12	0.1±0.04
57	o-Xylene	0.41±0.28	0.11±0.06	0.05±0.02
58	Styrene	0.39±0.31	0.03±0.01	0.01±0.01
59	Isopropylbenzene	0.04±0.02	-	0.01±0
60	Propylbenzene	0.04±0.02	0.02±0.01	0.01±0.01
61	n-Decane	0.09±0.07	0.15±0.07	0.02±0.01
62	1,3,5-Trimethylbenzene	0.06±0.04	0.02±0.01	0.01±0.01
63	1,2,4-Trimethylbenzene	0.16±0.12	0.06±0.02	0.02±0.01
64	1,2,3-Trimethylbenzene	-	0.1±0.03	-
65	Methane	2000.00[4]	2000.00[4]	2044.15±30.31
66	Formaldehyde	3.54±1.03	3.18±0[3]	4.93±1.53
67	Acetaldehyde	2.93±0.69	2.5±0[3]	2.17±0.52
68	Propionaldehyde	0.41±0.07	0.29±0[3]	0.17±0.07

69	Acetone	2.3±0.75	2.57±0[3]	5.11±1.7
70	Butyraldehyde	0.85±0.14	0.17±0[3]	1.5±0.47
71	Benzaldehyde	0.18±0.03	0.16±0[3]	0.11±0.03
72	n-Pentanal	0.27±0.04	0.04±0[2]	0.19±0.04
73	Hexanal	0.12±0	0.16±0[2]	0.13±0.04

[1] 24-h average values ± standard deviations are shown here. The units of VOCs and OVOCs are ppbv. "-" indicates that the parameter is not constrained in the model.

[2] The mixing ratio of this species is adopted from Gu et al. (2019).

[3] The mixing ratio of this species is adopted from Qian et al. (2019).

[4] The mixing ratio of this species is adopted from Tan et al. (2917).

Table S5. Comparison of the influencing factors of P(NO_3) in the winter and summer campaigns.

Place/Season	T (K)	k_1 (cm^3/molecule/s)	NO_2 (ppbv)	O_3 (ppbv)	[NO_2]×[O_3] ($molecule^2/cm^6$)	P(NO_3) (ppbv/h)
Wangdu						
Winter	271.8±3.2	$(1.5\pm0.2)\times10^{-17}$	34.1±13.0	4.7±4.5	$(0.9\pm0.7)\times10^{23}$	0.20±0.15
Summer	298.1±3.4	$(3.2\pm0.3)\times10^{-17}$	16.8±9.7	37.8±26.2	$(2.5\pm2.1)\times10^{23}$	1.34±1.09
Beijing						
Winter	270.3±3.7	$(1.4\pm0.2)\times10^{-17}$	27.9±19.1	14.5±11.5	$(1.5\pm1.0)\times10^{23}$	0.28±0.18
Early summer	295.3±4.5	$(3.0\pm0.4)\times10^{-17}$	23.6±13.6	27.2±20.6	$(2.9\pm2.4)\times10^{23}$	1.36±1.27
Mt. Tai						
Winter to early spring	277.1±5.8	$(1.8\pm0.3)\times10^{-17}$	2.0±1.7	65.1±14.1	$(0.8\pm0.6)\times10^{23}$	0.21±0.16
Summer	289.8±2.1	$(2.6\pm0.2)\times10^{-17}$	3.1±3.2	77.8±20.1	$(1.5\pm1.5)\times10^{23}$	0.56±0.55

Table S6. A summary of γ(N_2O_5) derived in the selected time periods of the winter campaigns.

Start Time	End Time	γ(N_2O_5)	φ($ClNO_2$)
Wangdu			
12/17/17 1:10	12/17/17 4:20	0.0150	0.037
12/24/17 23:40	12/25/17 1:30	0.0060	0.053
Beijing			
1/20/18 3:45	1/20/18 6:05	0.0075	0.630
1/25/18 23:40	1/25/18 2:20	0.0125	0.061
1/26/18 2:50	1/26/18 6:05	0.0149	0.038
Mt. Tai			
3/9/18 18:10	3/9/18 20:00	0.0525	0.797

3/24/18 19:20	3/24/18 21:00	0.0036	0.545
3/24/18 18:00	3/25/18 2:00	0.0060	0.179
3/25/18 21:00	3/26/18 2:00	0.0118	0.273

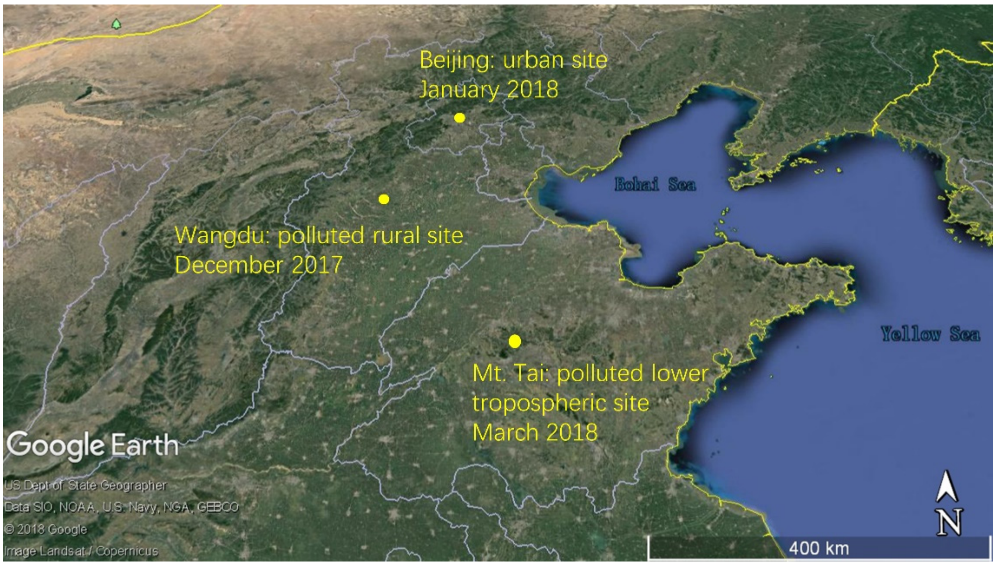

Figure S1. A map showing the three observation sites over the NCP.

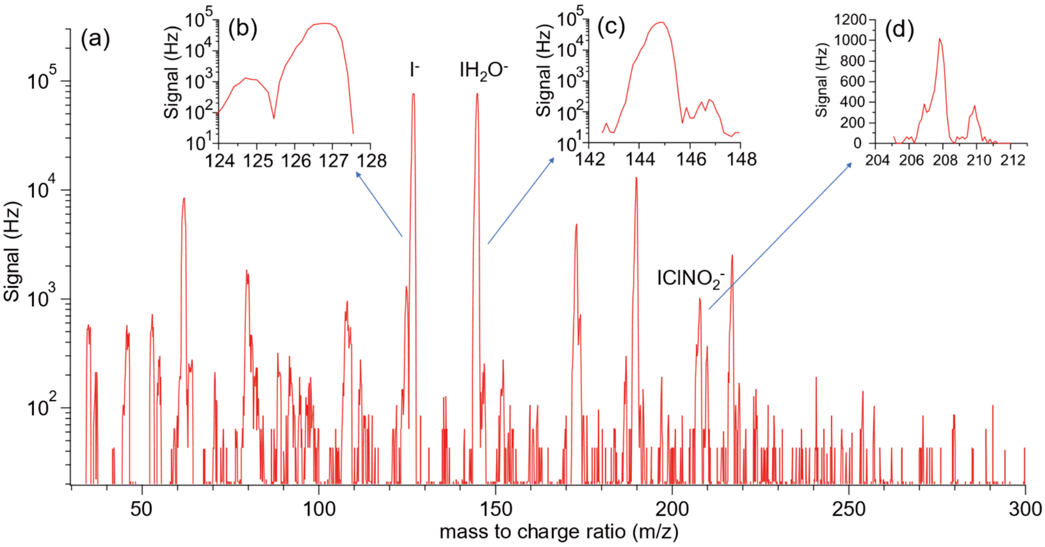

Figure S2. An example of the mass spectrum of Q-CIMS. **(a)** A full mass spectrum from 30 to 300 a.m.u. **(b)**, **(c)**, and **(d)** are expanded views of the mass spectrum for I^-, $I(H_2O)^-$, and $IClNO_2^-$, respectively.

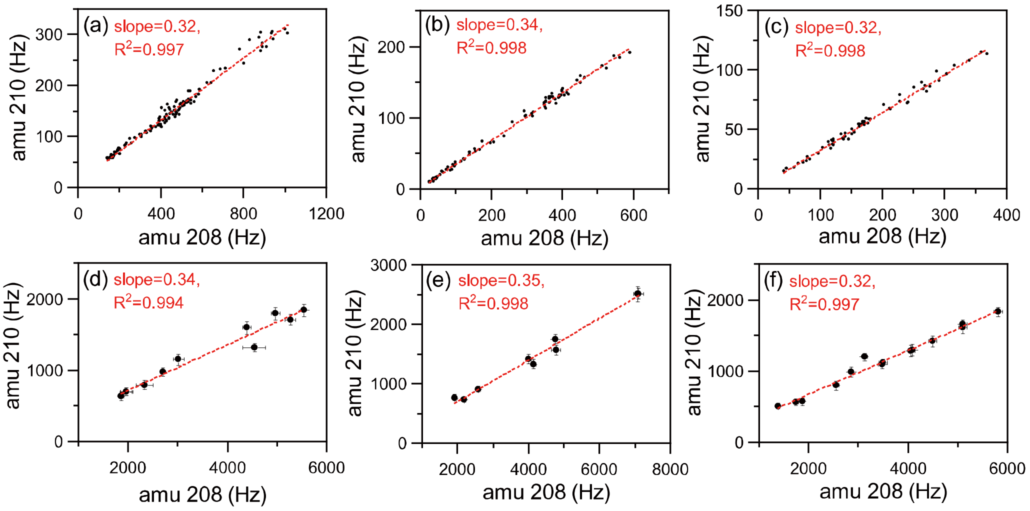

Figure S3. The signal of $I^{35}ClNO_2^-$ and $I^{37}ClNO_2^-$ during the ambient sampling and on-site calibrations. **(a)-(c)** represent the signals of 208 a.m.u. and 210 a.m.u. during the ambient observations on the daytime of 28 Dec 2017 in Wangdu, 14 January 2018 in Beijing, and 29 March 2018 in Mt. Tai, respectively. **(d)-(f)** show the respective signals of 208 a.m.u. and 210 a.m.u. during the on-site calibrations in Wangdu, Beijing, and Mt. Tai, respectively.

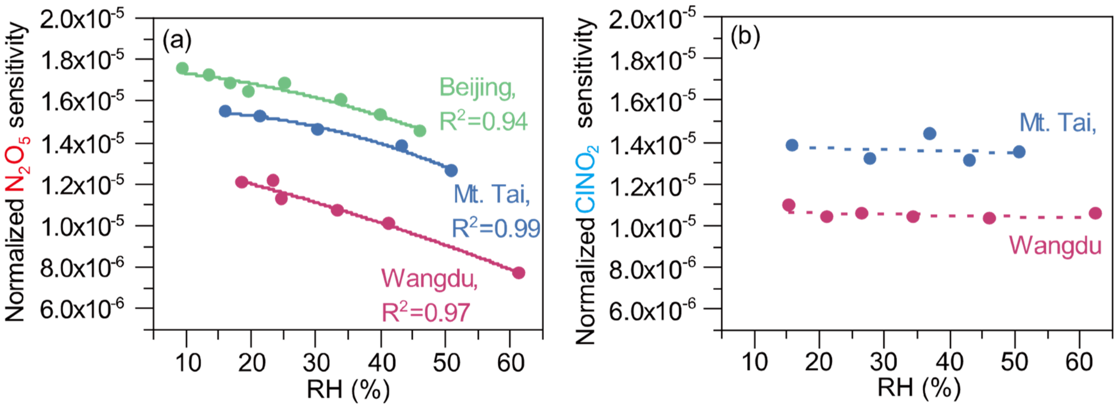

Figure S4. The dependence of normalized N_2O_5 and $ClNO_2$ sensitivities (unit: $pptv^{-1}$) on RH. The dots with different colors were experiment data in Wangdu, Beijing, and Mt. Tai, respectively. The N_2O_5 sensitivities were fitted by a quadratic function in the form of $y=ax^2+bx+c$.

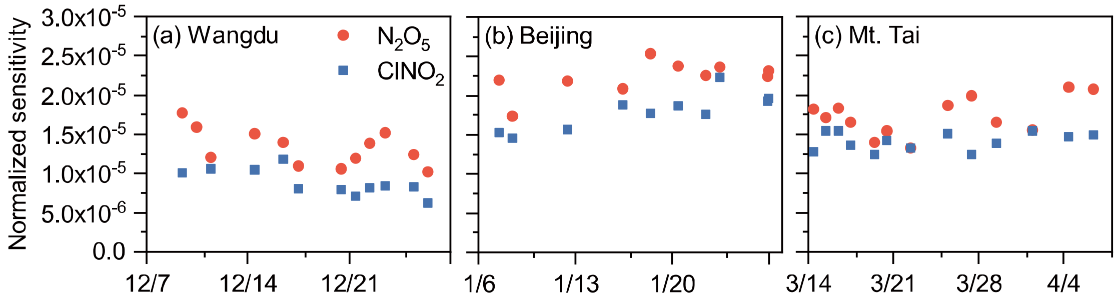

Figure S5. Summary of on-site calibrations of N_2O_5 and $ClNO_2$. The unit of the normalized sensitivity of N_2O_5 and $ClNO_2$ is $pptv^{-1}$.

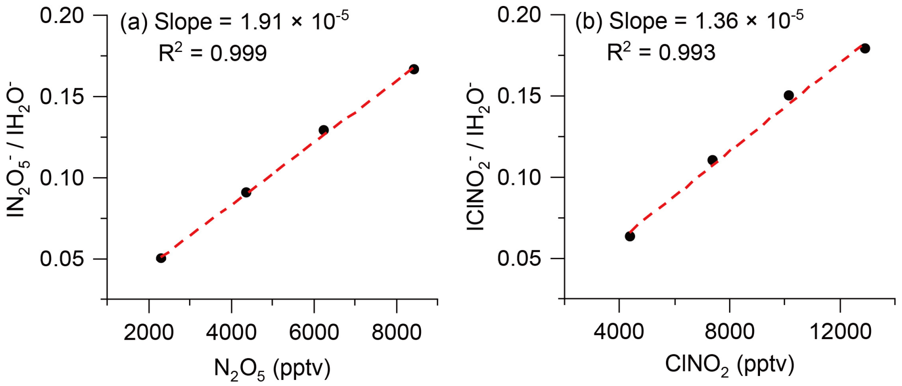

Figure S6. Multi-concentration calibrations of N_2O_5 and $ClNO_2$ conducted in the Mt. Tai campaign in March 2018.

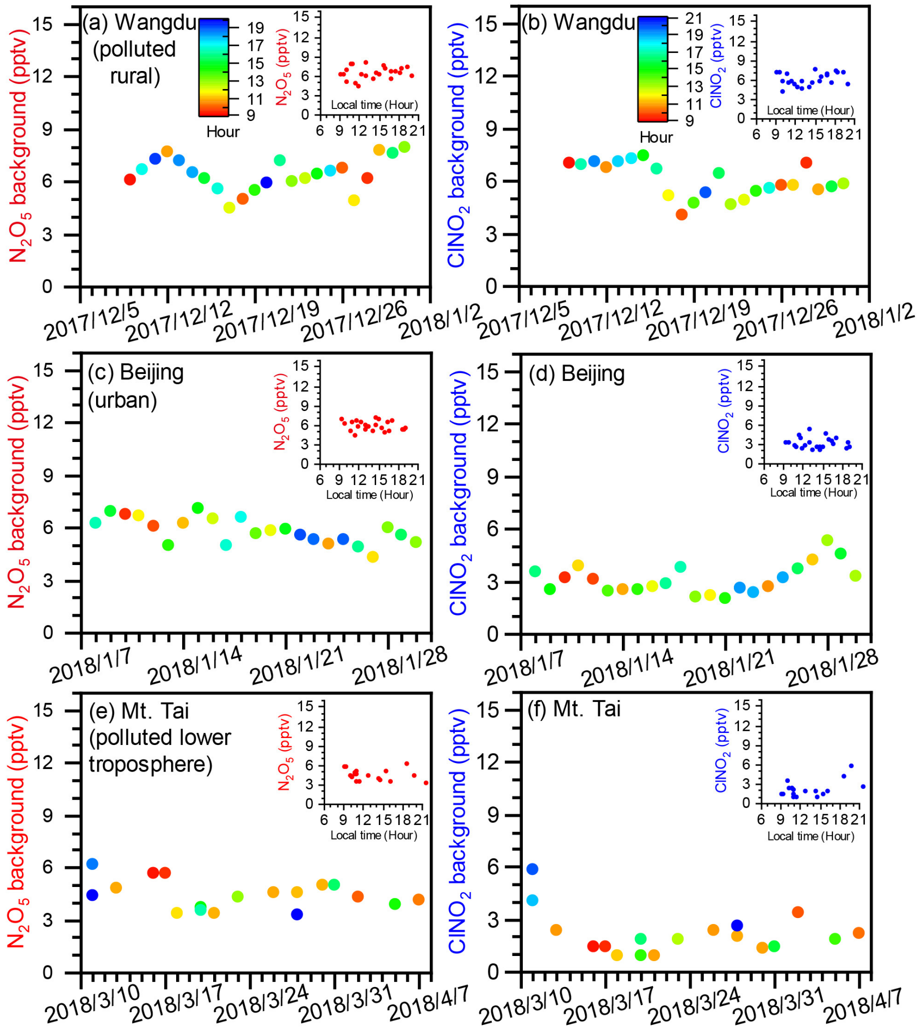

Figure S7. Background signals of N_2O_5 and $ClNO_2$ in the winter field campaigns over the NCP.

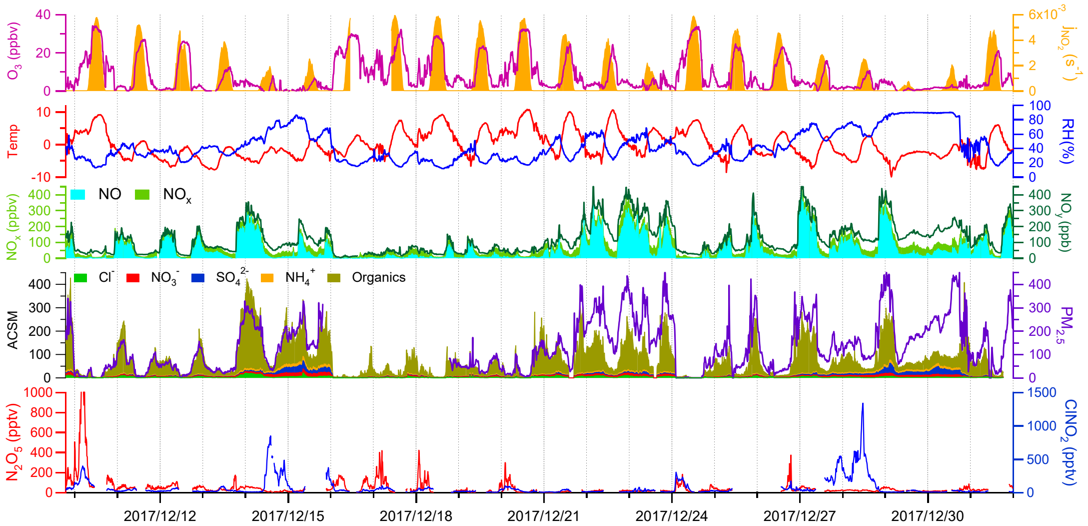

(a) Wangdu

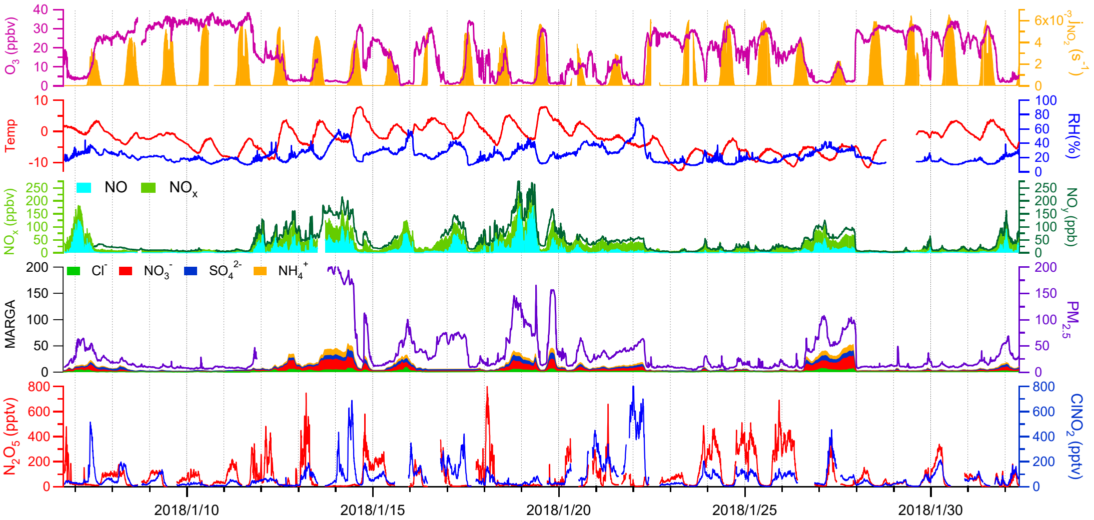

(b) Beijing

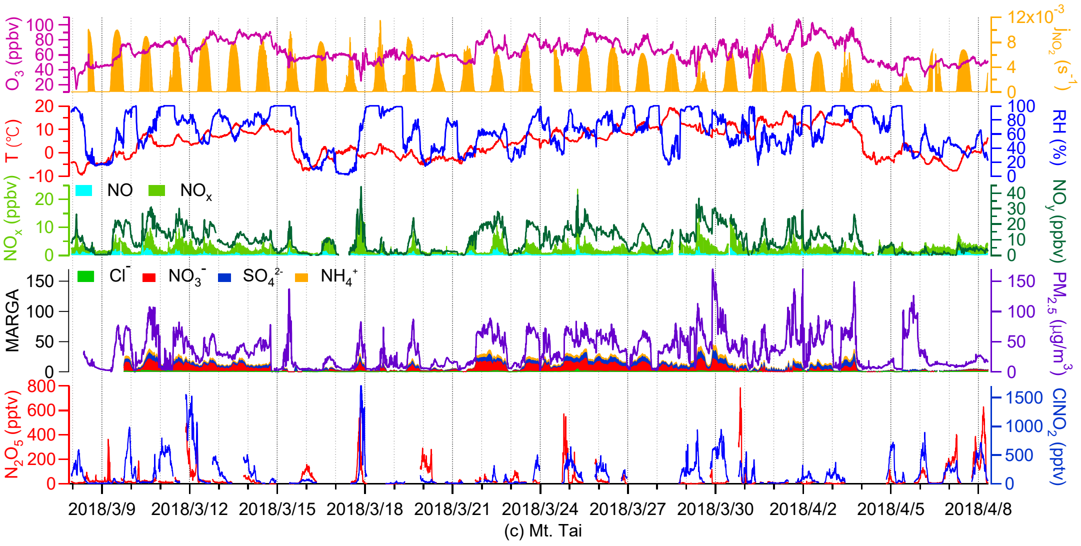

(c) Mt. Tai

Figure S8. Time series of some observed species in the winter campaigns. **(a)** the Wangdu campaign in December 2017, **(b)** the Beijing campaign in January 2018, and

(c) the Mt. Tai campaign in March 2018.

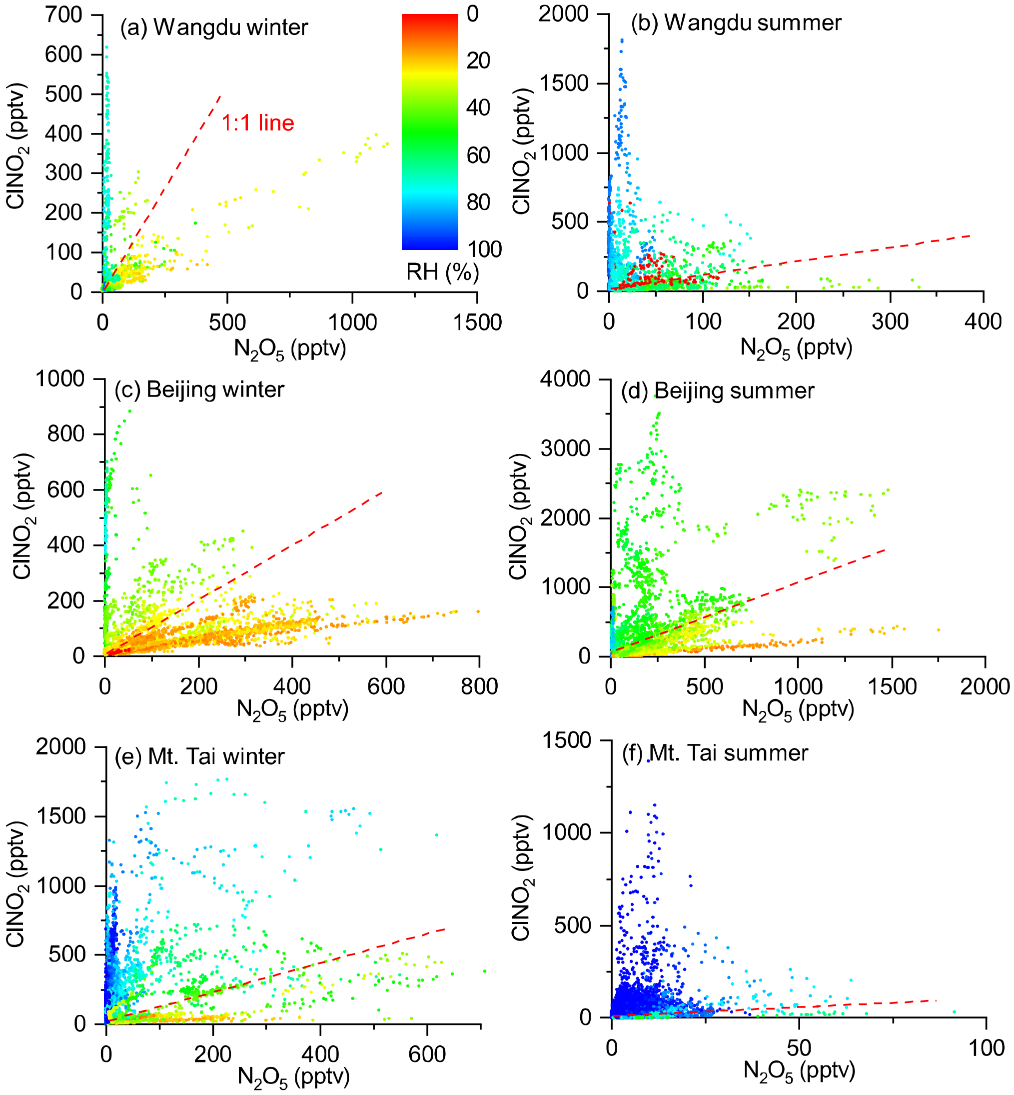

Figure S9. Nocturnal relationship of the concentrations of N_2O_5 and $ClNO_2$ in the winter and summer campaigns in Wangdu, Beijing, and Mt. Tai. The dashed line in red shows a 1:1 ratio of the concentrations of N_2O_5 and $ClNO_2$.

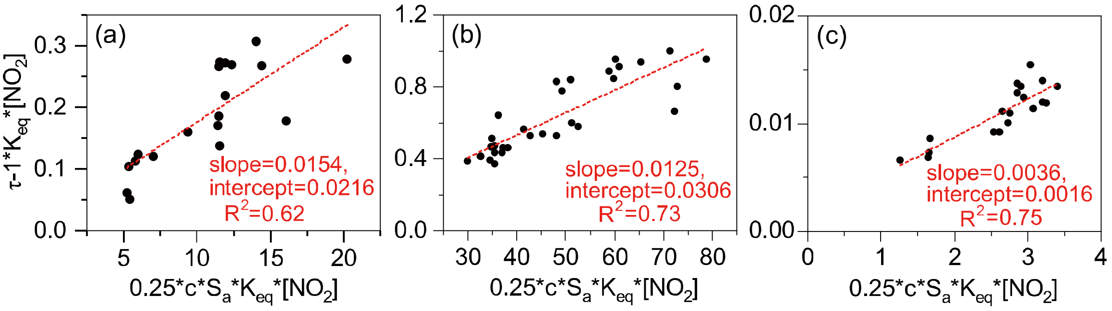

Figure S10. Examples of $\gamma(N_2O_5)$ derived using the steady-state method. **(a)** 16 December 2017 in Wangdu, **(b)** 25 January in Beijing, and **(c)** 24 March in Mt. Tai.

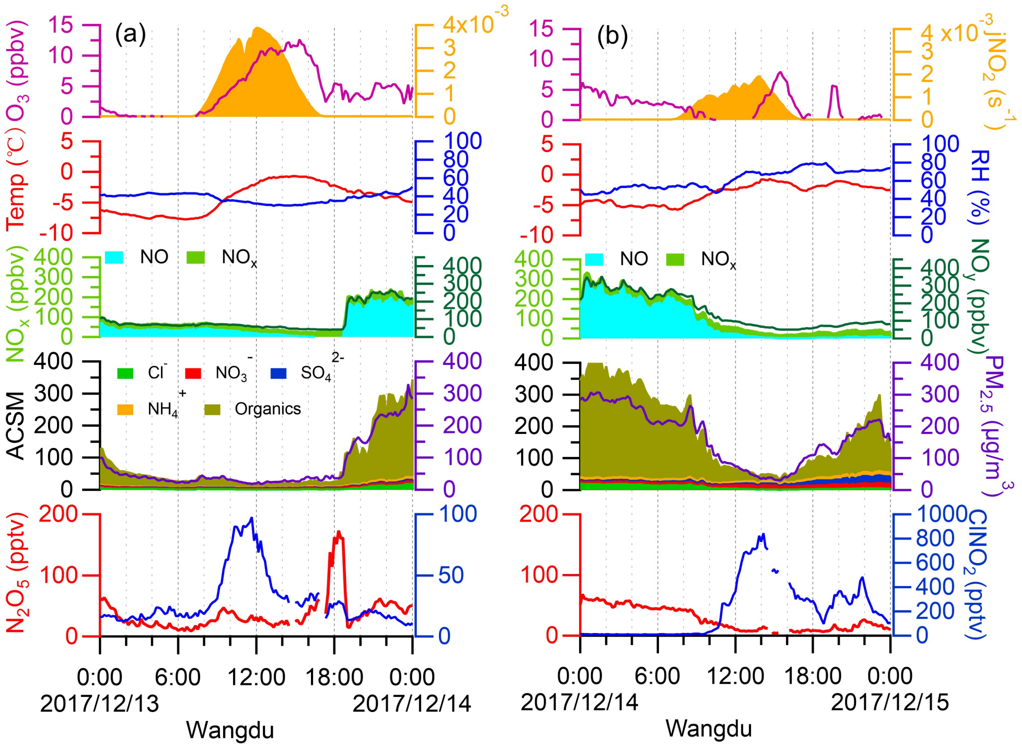

Figure S11. Examples of other daytime-ClNO2 cases observed during the winter Wangdu campaign.

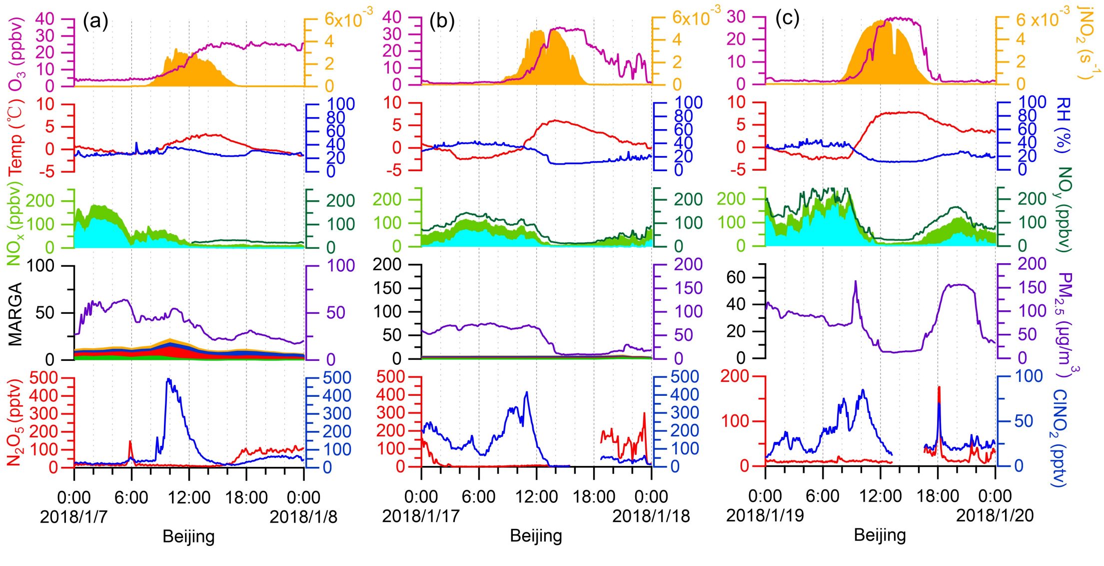

Figure S12. The same to Fig. S11 but for the winter Beijing campaign.

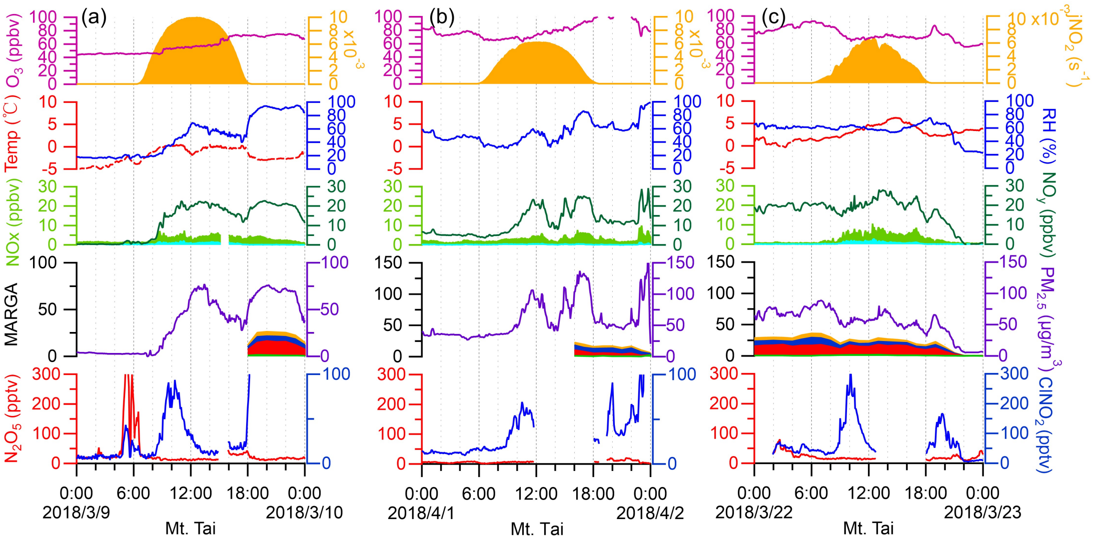

Figure S13. The same to Fig. S11 and Fig. S12 but for the winter Mt. Tai campaign.

References:

Veres, P. R., Neuman, J. A., Bertram, T. H., Assaf, E., Wolfe, G. M., Williamson, C. J., Weinzierl, B., Tilmes, S., Thompson, C. R., Thames, A. B., Schroder, J. C., Saiz-Lopez, A., Rollins, A. W., Roberts, J. M., Price, D., Peischl, J., Nault, B. A., Møller, K. H., Miller, D. O., Meinardi, S., Li, Q., Lamarque, J.-F., Kupc, A., Kjaergaard, H. G., Kinnison, D., Jimenez, J. L., Jernigan, C. M., Hornbrook, R. S., Hills, A., Dollner, M., Day, D. A., Cuevas, C. A., Campuzano-Jost, P., Burkholder, J., Bui, T. P., Brune, W. H., Brown, S. S., Brock, C. A., Bourgeois, I., Blake, D. R., Apel, E. C., and Ryerson, T. B.: Global airborne sampling reveals a previously unobserved dimethyl sulfide oxidation mechanism in the marine atmosphere, Proceedings of the National Academy of Sciences, 117, 4505-4510, 10.1073/pnas.1919344117, 2020.